Spring 5-18-2018

A Simulation Study of Bipower and Thresholded Realized Variations for High-Frequency Data

Zheng Xu
Washington University in St. Louis

WASHINGTON UNIVERSITY IN ST. LOUIS

Department of Mathematics

A Simulation Study of Bipower and Thresholded Realized Variations for High-Frequency Data

by

Zheng XU

A thesis presented to
The Graduate School
of Washington University in
partial fulfillment of the
requirements for the degree
of Master of Arts

May 2018
St. Louis, Missouri

Table of Contents

List of Figures

List of Tables

Table Page

Acknowledgments

I would like to thank my thesis adviser Professor, José E. Figueroa-López, for his patience and guidance in my research study. He teaches me a lot in the field of statistics and mathematical finance and always provides valuable suggestions in my research.

I would also like to thank my committee members Professor José E. Figueroa-López and Professor Nan Lin for their helpful advice and insightful comments.

My sincere thanks also goes to my wife Yifan Wang, my sister Siyang Xu, and my daughter Ningze Xu, for supporting me spiritually and providing me happiness in my life.

Finally, I wish to express my sincere gratitude to my parents, Yongxian Xu and Shuhua Jian, for their unfailing support and continuous encouragement throughout my life.

Zheng XU

Washington University in St. Louis

May 2018

Dedicated to my parents, my wife, my sister and my daughter.

ABSTRACT OF THE THESIS

A Simulation Study of Bipower and Thresholded Realized Variations for High-Frequency Data

by

XU, Zheng

A.M. in Statistics

Washington University in St. Louis, 2018

Professor José E. Figueroa-López, Chair

In the framework of general time-continuous stochastic models, multipower variation and threshold type variations are two popular nonparametric estimators with a wide range of applications. Given the high-frequency data, these methods aim to estimate the integrated volatility of the diffusion component in Itô type stochastic processes. In this thesis, we will focus on the bipower variation (BPV) and the thresholded realized variations (TRV) for some classical Lévy stochastic models. We use R to construct jump diffusion type models, the variance gamma model and the normal inverse Gaussian model and test the performance of estimators in each model with different time lags based on high-frequency data. We also introduce some types of threshold sequences that widely applied in the TRV estimators. Simulation results demonstrate that the TRV estimators with an optimal threshold sequence present a better performance on the efficiency of jump detection and accuracy of integrated volatility estimation in each model.

1. Introduction

1.1 Background

The Black-Scholes model is widely used to simulate a time-continuous stochastic process and model random behaviors in the financial market. Under the assumptions of the Black-Scholes model, the asset price is continuous without any jumps which is inconsistent with the data we obtained from the real market. Hence, it is difficult to use the Black-Scholes model to explain the phenomenon that an asset price changes by a relatively large amount within a small time interval, especially in the stock market. Expanding on the Black-Scholes model, the Merton jump diffusion model was proposed in which a finite number of jumps are superimposed on a continuous price process in a finite time interval [1]. Kou [2] also introduced a double exponential jump diffusion model, which aims to demonstrate the phenomenon of volatility smile and the leptokurtic features in asset pricing that the return distribution of assets may have a higher peak and heavier tails. Madan and Seneta [3] extended the Black-Scholes model by applying the variance gamma (VG) process to the jump part, which suggests that the increments of log-returns in the stock market follow a variance gamma distribution. Alternatively, Barndorff-Nielsen [4] developed the normal inverse Gaussian (NIG) Lévy model in which the inverse Gaussian distribution is employed into the jump component of a model for log-returns of asset prices. The Lévy models mentioned above incorporate market shocks, which lead to relatively sudden and large changes in asset prices in the financial market.

These kinds of price changes are difficult to be explained by the deviation of the diffusion component in the Black-Scholes model.

Based on simulations of each Lévy model, researches on the efficiency of jump detection and accuracy of integrated volatility estimation are conducted. In this paper, we aim to compare the accuracy of the BPV estimator and the TRV estimators for the integrated volatility estimation.

1.2 Basic theories of Lévy process

Definition 2.1 (Stochastic Process) [5]: *A stochastic process X on a probability space $(\Omega, \mathcal{F}, \mathbb{P})$ is a collection of random variables $(X_t)_{0 \leq t < \infty}$.*

Definition 2.2 (Brownian Motion) [5]: *Standard Brownian motion $W = (W_t)_{0 \leq t \leq \infty}$ satisfies the following three properties:*

- $W_0 = 0$.
- *W has independent increments: $W_t - W_s$ is independent of $\mathcal{F}_s$, $0 \leq s < t < \infty$.*
- *$W_t - W_s$ is a Gaussian random variable: $W_t - W_s \sim N(0, t-s) \, \forall \, 0 \leq s < t < \infty$.*

Definition 2.3 (Possion Process) [5]: *A Poisson process $N = (N_t)_{0 \leq t \leq \infty}$ satisfies the following three properties:*

- $N_0 = 0$.
- *N has independent increments: $N_t - N_s$ is independent of $\mathcal{F}_s$, $0 \leq s < t < \infty$.*
- *N has a stationary increments: $P(N_t - N_s \leq x) = P(N_{t-s} \leq x) \, \forall \, 0 \leq s < t < \infty$.*

Definition 2.4 (Lévy Process) [5]: *A cadlag stochastic process* $(X_t)_{t\geq 0}$ *on* $(\Omega, \mathcal{F}, \mathbb{P})$ *with value in* $\mathbb{R}^d$ *such that* $X_0 = 0$ *is called Lévy process if it follows three properties:*

- *Independent increments: for every increasing sequence of times* $t_0 \dots t_n$*, the random variables* $X_{t_0}, X_{t_1} - X_{t_0}, \dots, X_{t_n} - X_{t_{n-1}}$ *are independent.*
- *Stationary increments: the law of* $X_{t+h} - X_t$ *does not depend on* t*.*
- *Stochastic continuity:* $\forall \varepsilon > 0$, $\lim_{h\to 0} P(\mid X_{t+h} - X_t \mid > \varepsilon) = 0$.

2. Statistical models

In this chapter, we will introduce some types of jump diffusion models: the Merton jump diffusion model, the Kou model; and some Lévy processes building by Brownian subordination: the variance gamma model and the normal inverse Gaussian model. We will explain basic ideas of each model in detail and provide algorithms for data simulation in each model by R.

2.1 Jump diffusion model

2.1.1 Basic idea

The general jump diffusion model is defined as:

$$X_t := \gamma t + \sigma W_t + J_t = \gamma t + \sigma W_t + \sum_{j=1}^{N_t} \zeta_j. \tag{2.1}$$

The term of $\gamma t+\sigma W_t$ is a Brownian motion with drift process. The σ denotes the volatility of the diffusion component in the Brownian motion. The big difference between the Black-Scholes model and the general jump diffusion model is the jump term J_t: $\sum_{j=1}^{N_t} \zeta_j$ which is a compound Poisson jump process. A compound Poisson process is a continuous-time stochastic process with jumps. N_t is a Poisson process with the rate λ. The individual jumps $\zeta_j's$ are independently and identically distributed with the density f_ζ. We also assume that the jump density function is defined as:

$$f\left(x\right) = pf_+(x)\mathbf{1}_{[x\geq 0]} + \left(1-p\right) f_-\left(x\right) \mathbf{1}_{[x<0]}, \tag{2.2}$$

where $p \in [0,1]$, and $f_+ : [0,\infty) \to [0,\infty)$ and $f_- : (-\infty, 0] \to [0,\infty)$ are bounded density functions such that $f_\pm(0) := \lim_{x\to 0^\pm} f_\pm(x) \in (0,\infty)$.

The jump diffusion type model not only captures normal asset variations by the diffusion part of Brownian motion, but also illustrates the phenomenon of sudden and large jumps of asset prices by the Poisson-driven jump part in the financial industry. Popular examples of jump diffusion type models include the Merton jump diffusion model and the Kou model.

In the Merton model, jumps in the log-return X_t are assumed to follow a normal distribution: $\zeta_j \sim N(\mu, \delta^2)$ with the density function:

$$f_{Merton}(x) = \phi(\frac{x-\mu}{\delta})\frac{1}{\delta}, \tag{2.3}$$

where ϕ stands for the density of standard normal distribution, μ and δ represent the mean and standard deviation of the jump sizes. The main advantage of the Merton jump diffusion model is that it leads to heavier tails than the classical Black-Scholes model, which is better fit to the realistic data in the financial industry. Moreover, the Merton model can more precisely describe the implied volatility behavior in the real market. In the framework of the Black-Scholes model, the implied volatility should be maintained as a constant which contradicts the fact that the implied volatility varies in the realistic market. Figure 2.1 shows a sample path of an asset price driven by the Merton jump diffusion model with parameters: $\gamma = 0, \sigma = 0.4, \lambda = 100, \mu = 0, \delta = 0.03$.

In the Kou model, the jump sizes are modeled through an asymmetric double exponential distribution with the density function in the form of [2]:

$$f_{Kou}(x) = p\eta_1 e^{-\eta_1 x}\mathbf{1}_{\{x>0\}} + (1-p)\eta_2 e^{\eta_1 x}\mathbf{1}_{\{x<0\}}, \tag{2.4}$$

Figure 2.1. A sample path of an asset price driven by the Merton jump diffusion model with parameters: $\gamma = 0, \sigma = 0.4, \lambda = 100, \mu = 0, \delta = 0.03$.

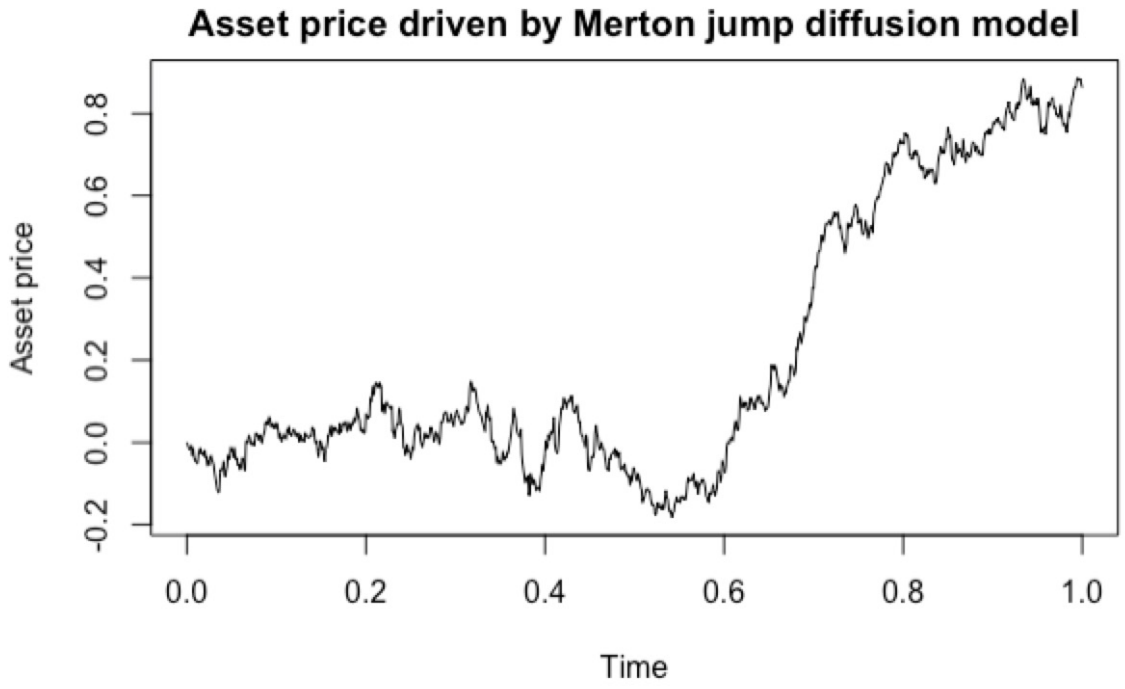

Figure 2.2. A sample path of an asset price driven by the Kou model with parameters: $\gamma = 0, \sigma = 0.4, \lambda = 100, p = 0.45, \eta_1 = 10, \eta_2 = 10$.

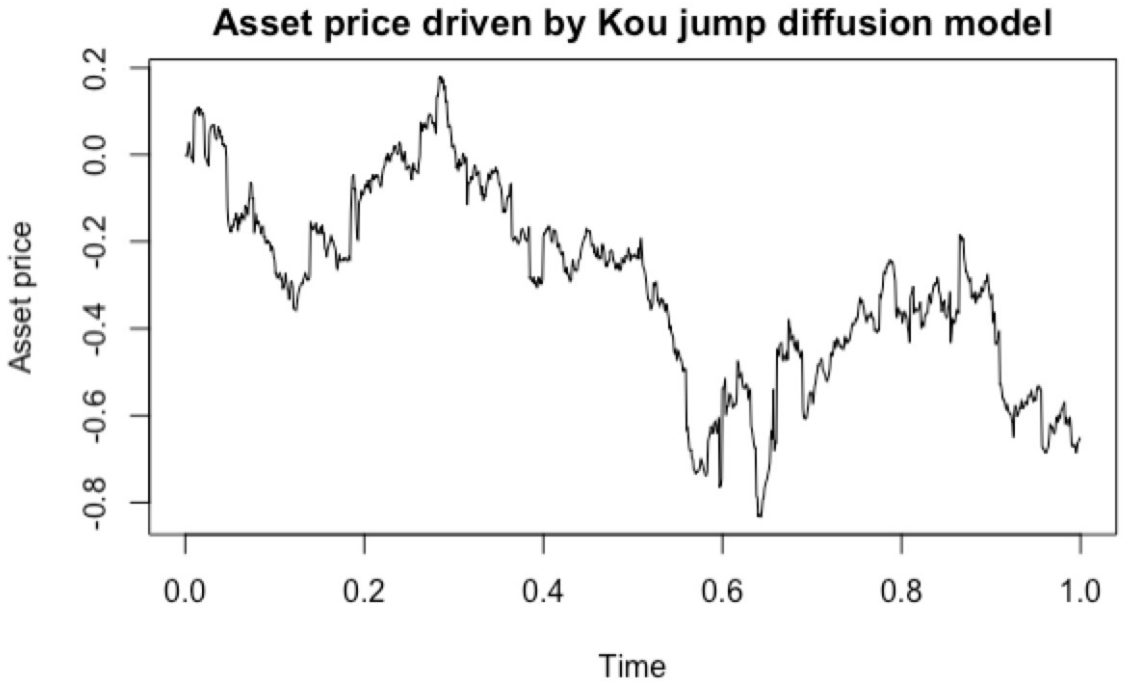

where $0 \leq p \leq 1$, $\eta_1 > 1$ and $\eta_2 > 0$. In this density function, p and $(1-p)$ represent the probabilities of the upward jumps and the downward jumps, respectively. In other words, jumps in the Kou model have the probability p to go upward in the size of ζ_{up} that randomly follows an exponential distribution with the mean of $1/\eta_1$ and the probability $(1-p)$ to go downward in the size of ζ_{down} that randomly follows an exponential distribution with the mean of $1/\eta_2$. Similar to the Merton model, the Kou model enables to demonstrate the leptokurtic features of a higher peak and heavier tails, and the curved implied volatility in the real financial market. Figure 2.2 is a sample path of the Kou model with parameters: $\gamma = 0, \sigma = 0.4, \lambda = 100, p = 0.45, \eta_1 = 10, \eta_2 = 10$.

2.1.2 Simulation algorithm

Assume we want to simulate a jump diffusion process with parameters γ, σ, λ. Let $t_1, t_2, \ldots, t_n$ be a set of equally spaced fixed time points, i.e., $\Delta = t_i - t_{i-1}$ where $t_0 = 0$, and $T = n\Delta$. A discretized trajectory of the general jump diffusion X without the drift process, say, $\gamma = 0$, is simulated by [5] :

- Simulate n normal variables, denoted as $G_i, \ldots, G_n$, with mean 0 and variance $\sigma\Delta$;
- Simulate a Poisson distributed random variable N with intensity parameter λT;
- Simulate N random variables τ_k that uniformly distributed in $[0, T]$; these variables correspond to the jump times;
- Simulate N random variables ζ_t that followed the distribution with density f_ζ, i.e. the normal distribution $N(0, \delta^2)$.

The discretized trajectory is then $Y_{t_i} = \sum_{i=1}^{n} G_i + \sum_{k=1}^{N} \mathbf{1}_{\{\tau_k < t_i\}} \zeta_k$.

2.2 Variance gamma model

2.2.1 Basic idea

In the variance gamma process, the time variables are randomly followed with a gamma distribution. The variance gamma model is defined as:

$$X_t = \gamma t + \sigma W_t + \sigma^{Jmp} B_{V_t} + \theta V_t, \tag{2.5}$$

where $\sigma, \sigma^{JMP} > 0$, $\gamma, \theta \in R$ are given constants, W and B are independent Wiener processes, V_t is gamma distributed with the shape parameter $\alpha = t/\kappa$ and the scale

parameter $\beta = \kappa$, and κ refers to the kurtosis in the log-returns distribution which controls the tail heaviness. Under the variance gamma model, the log-returns follow the normal distribution depending on the realization of a random time variable which is distributed from a gamma process. The appealing feature of the variance gamma model includes that the kurtosis parameter κ could result in a symmetric increase in both of the left and right tail probabilities of the log-returns distribution [3].

2.2.2 Simulation algorithm

Assume we want to simulate a variance gamma process with parameters $\gamma, \sigma, \sigma^{JMP}, \theta, \kappa$, and to be simplified, we set $\gamma = 0$. A discretized trajectory of the variance gamma process of $(X(t_1), \ldots, X(t_n))$ for equally spaced fixed times $t_1, \ldots, t_n$ in which $\Delta = t_i - t_{i-1}$ and $t_0 = 0$ can be generated as follows [5]:

- Generate n normal variables, denoted as $G_i, \ldots, G_n$, with mean 0 and variance $\sigma\Delta$;
- Generate n independent gamma variables $\Delta S_1, \ldots, \Delta S_n$ with parameters $\frac{\Delta}{\kappa}$ and κ;
- Set $\Delta S_i = \kappa \Delta S_i$ for all i;
- Generate n random variables $N_1, \ldots, N_n$ that independently and identically follow the normal distribution $N(0, 1)$;
- Set $\Delta X_i = G_i + \sigma^{JMP} N_i \sqrt{\Delta S_i} + \theta \Delta S_i$ for all i.

The trajectory is given by: $X(t_i) = \sum_{k=1}^{i} \Delta X_i$. Figure 2.3 shows a sample path of an asset price driven by the variance gamma model with parameters: $\gamma = 0, \theta = 0, \sigma = 0.4, \sigma^{JMP} = 0.03, \kappa = 0.3$.

Figure 2.3. A sample path of an asset price driven by the variance gamma model with parameters: $\gamma = 0, \theta = 0, \sigma = 0.4, \sigma^{JMP} = 0.03, \kappa = 0.3$.

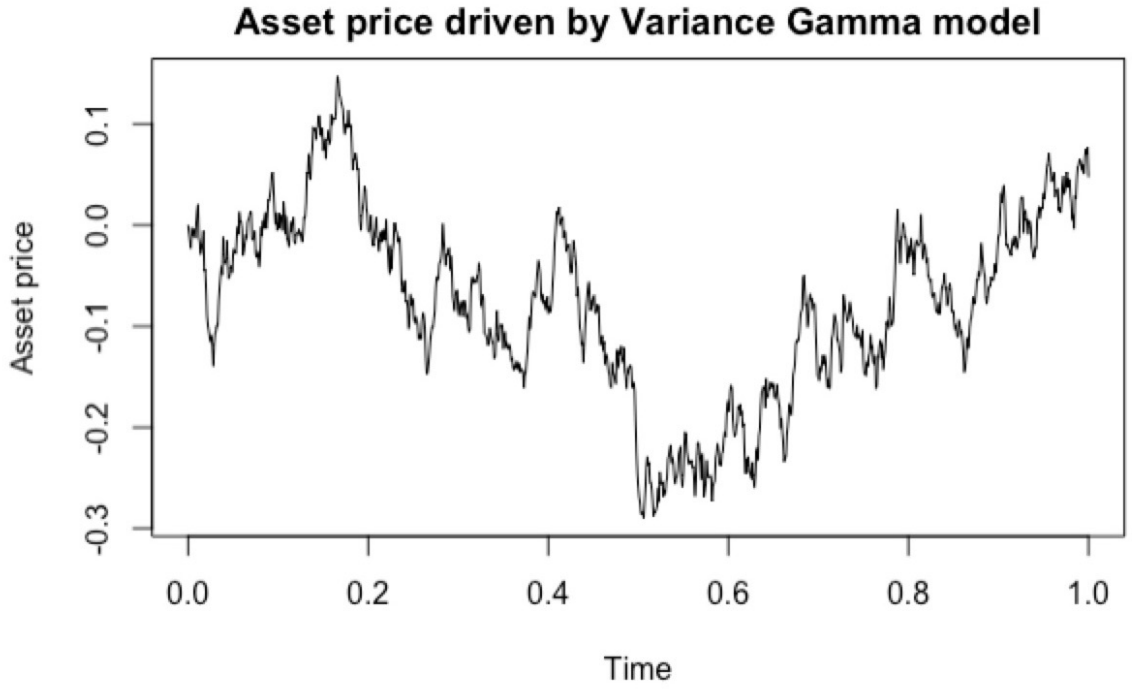

2.3 Normal inverse Gaussian model

2.3.1 Basic idea

In the normal inverse Gaussian process, the time variables are randomly followed with an inverse Gaussian distribution. The normal inverse Gaussian model is defined as:

$$X_t = \gamma t + \sigma W_t + \sigma^{Jmp} B_{I_t} + \theta I_t, \tag{2.6}$$

where $\sigma, \sigma^{JMP} > 0$, $\gamma, \theta \in R$ are given constants, W and B are independent Wiener processes, and I_t follows an inverse Gaussian distribution with parameters $\mu = t$ and $\lambda = t^2/\kappa$. Similar to the gamma variance model, the normal inverse Gaussian process is able to model asymmetric behaviors of the log-returns distribution and leads to semi-heavy tails of the return density.

2.3.2 Simulation algorithm

Suppose we want to simulate a normal inverse Gaussian process with parameters $\gamma, \sigma, \sigma^{JMP}, \theta, \kappa$, and we also assume that $\gamma = 0$. A discretized trajectory of the normal inverse Gaussian process of $(X(t_1), \ldots, X(t_n))$ for equally spaced fixed times $t_1, \ldots, t_n$ where $\Delta = t_i - t_{i-1}$ and $t_0 = 0$ can be simulated as follows [5]:

- Generate n normal variables, denoted as $G_i, \ldots, G_n$, with mean 0 and variance $\sigma\Delta$;
- Generate n independent inverse Gaussian variables $\Delta S_1, \ldots, \Delta S_n$ with parameters Δ and $\frac{\Delta^2}{\kappa}$;

Figure 2.4. A sample path of an asset price driven by the normal inverse Gaussian model with parameters: $\gamma = 0, \theta = 0, \sigma = 0.4, \sigma^{JMP} = 0.03, \kappa = 0.3$.

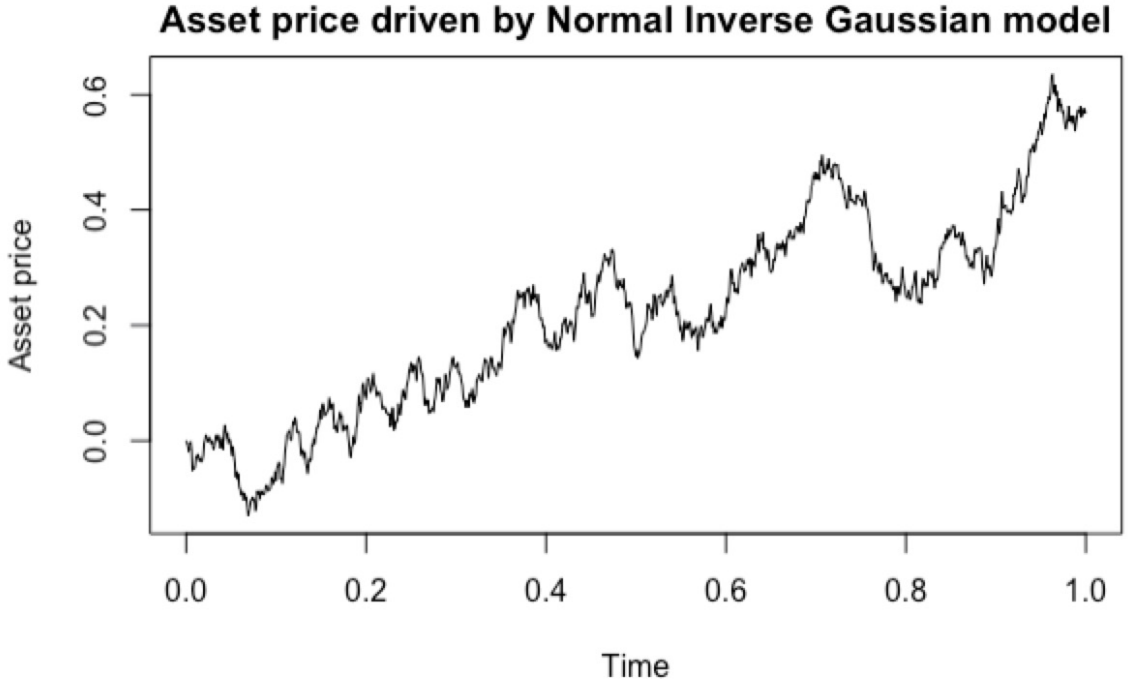

- Generate n random variables $N_1, \ldots, N_n$ that independently and identically follow the normal distribution $N(0, 1)$;
- Set $\Delta X_i = G_i + \sigma^{JMP} N_i \sqrt{\Delta S_i} + \theta \Delta S_i$ for all i.

The trajectory is given by: $X(t_i) = \sum_{k=1}^{i} \Delta X_i$. Figure 2.4 shows a sample path of an asset price driven by the normal inverse Gaussian model with parameters: $\gamma = 0, \theta = 0, \sigma = 0.4, \sigma^{JMP} = 0.03, \kappa = 0.3$.

3. Methods of estimating integrated volatility

In this chapter, we introduce some nonparametric estimators for the integrated volatility $\int_0^T \sigma_s^2 ds$ of a general Lévy process in the form of:

$$X_t = \int_0^t \gamma_s ds + \int_0^t \sigma_s dW_s + J_s, \tag{3.1}$$

where J is a pure jump process. Most commonly used nonparametric estimators fall into two classes: multipower and threshold type estimators. In this paper, we will focus on the bipower variation method and the thresholded realized variations method. We now proceed to give their definitions, properties and heuristic descriptions of their mechanics, respectively.

3.1 Bipower variation (BPV) estimator

3.1.1 Motivation

The bipower variation estimator (BPV) is the simplest form of multipower variation estimator, which was introduced by Barndorff-Nielsen and Shephard [6]. Given the consecutive increments $X_\Delta - X_0, \ldots X_{n\Delta} - X_{(n-1)\Delta}$ of X where $X_0 = 0$, the BPV estimator of integrated volatility σ is estimated through the formula

$$\hat{\sigma}^2_{BPV} = \frac{1}{T} BPV\,(X)^n_t \tag{3.2}$$

$$= \frac{\pi}{2T} \sum_{i=1}^{n-1} |X_{i\Delta} - X_{(i-1)\Delta}| \cdot |X_{(i+1)\Delta} - X_{i\Delta}|, \tag{3.3}$$

where $T = n\Delta$ and

$$BPV\,(X)_t^n = \frac{\pi}{2}\sum_{i=1}^{n-1}|X_{i\Delta} - X_{(i-1)\Delta}| \cdot |X_{(i+1)\Delta} - X_{i\Delta}|. \tag{3.4}$$

The BPV estimator is inspired by the traditional realized quadratic variation (QV)

$$QV(X)_t^n = \sum_{i=1}^{n}|X_{i\Delta} - X_{(i-1)\Delta}|^2, \tag{3.5}$$

which, as $\Delta \to 0$, satisfies

$$\sum_{i=1}^{n}|X_{i\Delta} - X_{(i-1)\Delta}|^2 \to \int_0^T \sigma_s^2 ds + \sum_{j=1}^{N_T}\zeta_j^2.$$

For a continuous process, the realized quadratic variation estimator is a good estimate of the integrated volatility $\int_0^T \sigma_s^2 ds$. However, the QV estimator cannot estimate $\int_0^T \sigma_s^2 ds$ anymore when the model incorporates the jump component. This is because the QV estimator not only contains the integrated volatility $\int_0^T \sigma_s^2 ds$ but also includes the sum of the squared value of the increments that are driven by the jump component, say, $\sum_{j=1}^{N_T}\zeta_j^2$.

To solve the infeasibility of the QV estimator for the jump diffusion type models, the BPV estimator was proposed and was considered as a good estimate of the integrated volatility. We first assume that there is at least one big jump in $[(i-1)\Delta, (i+1)\Delta]$, and we also suppose that it is unlikely two such jumps would occur in two adjacent intervals. Under these assumptions, we find that $|X_{i\Delta} - X_{(i-1)\Delta}| \cdot |X_{(i+1)\Delta} - X_{i\Delta}|$ is approximately equal to 0, which effectively eliminates the influence of the jump part on integrated volatility estimation. In addition, the quadratic variation can be approximately estimated through

$$|X_{i\Delta} - X_{(i-1)\Delta}| \cdot |X_{(i+1)\Delta} - X_{i\Delta}| \approx \left(X_{i\Delta} - X_{(i-1)\Delta}\right)^2. \tag{3.6}$$

Thus, the bipower variation method could result in a more accurate estimation of the integrated volatility. Furthermore, the constant coefficient $\pi/2$ in the BPV estimator,

which is obtained by $\mathbb{E}\left(\mid Z \mid\right)^{-2}$ for a standard Gaussian variable Z, makes the estimator unbiased and consistent.

The appealing advantage of the bipower variation method is that it is easy to implement in practice since we can directly substitute the data we have to estimate the $\int_0^T \sigma_s^2 ds$ without any other parameters. However, for lower order of the multipower variation estimator, for instance the BPV estimator, can exhibit higher levels of bias and variability in the presence of jumps, even for a reasonably large sample size.

3.1.2 Properties

Under the framework of a Finite-Jump Activity (FJA) additive process X_t that in the form of (3.1) with the jump density function (2.2), the bias and variance of the BPV estimator relative to the parameter σ^2 take the following expressions (see [7] for details):

$$\mathbb{E}\left[BPV\left(X\right)_T^n\right] - T\sigma^2 \sim 2T\sigma\lambda\mathbb{E}\left[\left|\zeta_1\right|\right] m_1^{-1}\Delta^{1/2}, \tag{3.7}$$

$$Var\left(BPV\left(X\right)_T^n\right) \sim T\left\{\sigma^4\left(1+2m_1^2-3m_1^4\right)+2\sigma^2\lambda\left(1+m_1^2\right)\mathbb{E}\left[\zeta_1^2\right]+\left(\lambda\mathbb{E}\left[\zeta_1^2\right]\right)^2\right\} m_1^{-4}\Delta \tag{3.8}$$

where ζ_1 refers to a realization of a jump with the density function f_ζ, and $m_1 = \mathbb{E}\left[\mid Z \mid\right] = \sqrt{2/\pi}$ for a standard Gaussian random variable Z.

3.2 Thresholded realized variations (TRV) estimator

3.2.1 Motivation

The thresholded realized variations (TRV) method was introduced by Mancini [8] [9]. Given that a threshold sequence $\mathbf{B} = (B_n)_{n\geq 1}$ such that $B_n > 0$ and $\lim_{n\to\infty} B_n = 0$, the integrated variance σ is estimated by

$$\hat{\sigma}^2_{TRV} = \frac{1}{T} TRV(X)[B_n]^n_t \tag{3.9}$$

$$= \frac{1}{T}\sum_{i=1}^{n} |X_{i\Delta} - X_{(i-1)\Delta}|^2 \cdot \mathbf{1}_{\left\{|X_{i\Delta}-X_{(i-1)\Delta}|\leq B_n\right\}}. \tag{3.10}$$

The basic idea of the TRV method for estimating σ is to identify the large increments during the small interval, which may be caused by the jumps or market shocks during that time. Once the large increment has been identified by the threshold, it can be discarded in order to exclude the effects of the jump component, so that we can obtain a more accurate result for estimating the diffusion coefficient σ. In addition to obtaining the increments X_Δ, $X_{2\Delta-\Delta}$, $X_{3\Delta-2\Delta}$, $\ldots$, $X_{n\Delta-(n-1)\Delta}$, the main task of the TRV method is to find a proper threshold B_n that significantly influences the efficiency of the jump detection.

3.2.2 Properties

In the framework of a Lévy process X in the form of (2.1) with the jump density function (2.2), and given that a positive threshold sequence $\mathbf{B} = (B_n)_{n\geq 1}$ such that

$\lim_{n\to\infty} B_n = 0$, the bias and variance of the TRV estimator relative to the parameter σ^2 take the following expressions (see [7] for details):

$$\mathbb{E}\left[TRV(X)[B]_T^n\right] - T\sigma^2 = -2T\sigma\phi\left(\frac{B_n}{\sigma_n}\right)\left(\frac{B_n}{\Delta^{\frac{1}{2}}}\right) + T\Delta\left(\gamma^2 - \lambda\sigma^2\right) + \frac{2}{3}T\lambda\mathcal{C}_0\left(f\right)B_n^3 + h.o.t., \tag{3.11}$$

$$\mathrm{Var}(TRV(X)[B]_T^n) = 2T\sigma^4\Delta + \frac{2}{5}T\lambda B_n^5\mathcal{C}_0\left(f\right) + h.o.t., \tag{3.12}$$

where $\phi(\cdot)$ refers to the density function of standard Gaussian distribution, $\mathcal{C}_0(f) := \frac{1}{2}[pf_+(0) + (1-p)f_-(0)]$, $\sigma_n^2 = \frac{\sigma^2}{n}$, and $h.o.t$ is defined as "higher order terms."

4. Monte Carlo study

4.1 Estimation methods of the threshold

Not all sequence $\mathbf{B} = (B_n)_{n\geq 0}$ of positive elements converging to 0 as $n \to \infty$ will be a suitable threshold for the threshold type estimators. In the literature, several selection methods for the threshold sequence B have been proposed.

Mancini proposed a power threshold in the form of [9] :

$$B_n \left[Pow \left(\alpha, \omega \right) \right] = \alpha \Delta^{\omega}, \tag{4.1}$$

for some constant $\alpha > 0$ and $\omega \in \left(0, \frac{1}{2}\right)$. In recent work, Jacod and Todorov [10] set $\alpha = 4\hat{\sigma}_{BPV}$ and $\omega = 0.49$. We denote the TRV estimator with this specific threshold as $\hat{\sigma}^2_{TRV_{JT}}$ in our simulation experiments.

Figueroa-López and Mancini [11] developed an optimal threshold sequence selection method for the TRV method, which aims to minimize the mean square error (MSE) of the TRV estimator $I\hat{V}_n$ of the integrated variance $IV := \int_0^T \sigma_s^2 ds$. The MSE function is defined in the form of:

$$MSE := \mathbb{E}\left[(I\hat{V}_n - IV)^2 \right], \tag{4.2}$$

where

$$I\hat{V}_n := \sum_{i=1}^{n} \mid X_{i\Delta} - X_{(i-1)\Delta} \mid^2 \cdot \mathbf{1}_{\left\{ |X_{i\Delta} - X_{(i-1)\Delta}| \leq B_n \right\}}, \tag{4.3}$$

for a fixed time horizon $[0, T]$ with the equally spaced time interval $\Delta = \frac{T}{n}$. We first assume that there exist some large jumps in the model, then the threshold sequence $\mathbf{B}$

can be considered a significant factor in determining the value of the MSE function. For instance, $B_n = 0$ will result in $\hat{IV}_n = 0$ and then $MSE = \mathbb{E}[IV^2]$; as the threshold sequence B_n increases, the value of the MSE decreases for the reason that $\hat{IV}_n$ contains some squared increments $\mid X_{i\Delta} - X_{(i-1)\Delta}|^2$ and becomes closer to IV; however, when B_n approaches an extremely large number, say, infinity, the quantity of the MSE increases to $\mathbb{E}[(\sum_{i=1}^{n} \mid X_{i\Delta} - X_{(i-1)\Delta}|^2)^2]$ since $\hat{IV}$ includes all squared increments $\mid X_{i\Delta} - X_{(i-1)\Delta}|^2$ and equals to $IV + \sum_{i=1}^{n} \mid X_{i\Delta} - X_{(i-1)\Delta}|^2$. Therefore, if we aim to estimate the integrated volatility IV in the Lévy type model, a feasible method comes to mind which focuses on finding an optimal threshold $\mathbf{B}^*$ such that

$$MSE(\mathbf{B}^*) = \min_{\mathbf{B}\in[0,\infty)} MSE(\mathbf{B}). \tag{4.4}$$

In addition, an optimal threshold $\mathbf{B}^*$ should satisfy:

$$\lim_{n\to\infty} B_n \to 0 \quad and \quad \lim_{\Delta\to 0} \frac{B_n^*}{\sqrt{\Delta}} \to \infty.$$

Through the asymptotic behavior of $\mathbf{B}^*$ based on high-frequency data, we find an optimal threshold in the form of (see [11] for details):

$$B_n^* \sim \sqrt{2\hat{\sigma}^2 \Delta \ln\left(\frac{1}{\Delta}\right)},\ as\ \Delta \to 0.$$

Figueroa-López and Nisen [12] also introduced an applicable selection criterion for the threshold $\mathbf{B}$, which aims to minimize the statistical loss function of the total numbers of jump missclassifications for a fixed time horizon $T > 0$, and the equal time lag $\Delta = \frac{T}{n}$. To be more specific, there are two types of jump misclassifications: the increment $X_{i\Delta} - X_{(i-1)\Delta}$ does not contain any jumps but still exceeds the corresponding threshold in absolute value, i.e., the indicator function $\mathbf{1}_{\left[|X_{i\Delta}-X_{(i-1)\Delta}|>B_n, N_{i\Delta-(i-1)\Delta}=0\right]}$ is one; or the

increment $X_{i\Delta} - X_{(i-1)\Delta}$ involves at least one jump but fails to exceed the corresponding threshold in magnitude, i.e., the indicator $\mathbf{1}_{\left[|X_{i\Delta}-X_{(i-1)\Delta}|\leq B_n, N_{i\Delta-(i-1)\Delta}\neq 0\right]}$ is one. We set the loss function of the total numbers of jump missclassifications as:

$$Loss_n(\mathbf{B}) := \mathbb{E}\left[\sum_{i=1}^{n}(\mathbf{1}_{\left[|X_{i\Delta}-X_{(i-1)\Delta}|> B_n, N_{i\Delta-(i-1)\Delta}=0\right]} + \mathbf{1}_{\left[|X_{i\Delta}-X_{(i-1)\Delta}|\leq B_n, N_{i\Delta-(i-1)\Delta}\neq 0\right]})\right]. \tag{4.5}$$

If we could figure out the jump missclassifications problems in the model and minimize the total numbers of the jump misclassifications, in other words, minimize the loss function in the form of (4.5), we could obtain a relatively proper threshold $\mathbf{B}^*$ for the integrated volatility estimation such that

$$Loss_n(\mathbf{B}^*) = \min_{\mathbf{B}\in[0,\infty)} Loss_n(\mathbf{B}). \tag{4.6}$$

According to [12], for a fixed time horizon $T > 0$ with the equal small time lag Δ such that $\Delta = \frac{T}{n}$, an optimal threshold obtained by minimizing total numbers of jump misclassifications is in the form of: $\sqrt{3\hat{\sigma}^2\Delta \ln\left(\frac{1}{\Delta}\right)}$.

4.2 Simulation performances

In the simulation experiments, we consider the following estimators that we have mentioned before:

1. The BPV estimator $\hat{\sigma}^2_{BPV}$;
2. The TRV estimator $\hat{\sigma}^2_{TRV_{JT}}$ given using a threshold of the form $B_n = 4\Delta^{0.49}\hat{\sigma}_{BPV}$;
3. The TRV estimator $\hat{\sigma}^2_{TRV,2mc}$ given using a threshold of the form $B_n = \sqrt{2\hat{\sigma}^2\Delta \ln\left(\frac{1}{\Delta}\right)}$;
4. The TRV estimator $\hat{\sigma}^2_{TRV,3mc}$ given using a threshold of the form $B_n = \sqrt{3\hat{\sigma}^2\Delta \ln\left(\frac{1}{\Delta}\right)}$.

4.2.1 Simulation algorithm

We take $B_n = \sqrt{3\hat{\sigma}^2 \Delta ln\left(\frac{1}{\Delta}\right)}$ as an example and use the following algorithm which was first introduced in [12] to estimate the σ:

1. Assign an initial value for σ, say, $\hat{\sigma}_0 = \hat{\sigma}_{TRV}\,(B_n = \infty)$;
2. Roughly estimate the initial value of B_0^* through the formula $B_0^* = \sqrt{3\hat{\sigma}_0 \Delta ln\left(\frac{1}{\Delta}\right)}$;
3. Estimate the σ using B_0^*, then we have $\hat{\sigma}_1 = \hat{\sigma}_{TRV}\,(B_0^*)$;
4. Update B_1^* using $\hat{\sigma}_1$ by the formula $B_1^* = \sqrt{3\hat{\sigma}_1^2 \Delta ln\left(\frac{1}{\Delta}\right)}$, and so forth until $\mathbf{B}^*$ converges.

4.2.2 Simulation results

The adopted time unit of measure is 1 year (252 days). We consider 1-minute, 5-minute, 10-minute, 30-minute observations over a 1-month time horizon with a 6.5-hour per day open market, that is,

$$\begin{aligned}
\Delta_{1min} &= \frac{1}{252 \times 6.5 \times 12 \times 5}, \\
\Delta_{5min} &= \frac{1}{252 \times 6.5 \times 12}, \\
\Delta_{10min} &= \frac{1}{252 \times 6.5 \times 6}, \\
\Delta_{30min} &= \frac{1}{252 \times 6.5 \times 2}.
\end{aligned}$$

In the Merton model simulation experiments, the following parameters are used:

$$\gamma = 0, \sigma = 0.4, \mu^{JMP} = 0, \sigma^{JMP} = 3\sqrt{\Delta}, \lambda = 100.$$

Additionally, we believe that the rate of λ plays an important role in precisely estimating the integrated volatility, so we choose a relatively smaller amount and a relatively larger

Table 4.1
Estimates of mean σ for the Merton jump diffusion model with $\lambda = 10$ based on $K = 1000$ sample paths

Δ	$\mathbb{E}(\hat{\sigma}_{BPV})$	$\mathbb{E}(\hat{\sigma}_{TRV_{JT}})$	$\mathbb{E}(\hat{\sigma}_{TRV,2mc})$	$\mathbb{E}(\hat{\sigma}_{TRV,3mc})$
1 min	0.4002556	0.3999997	0.4000695	0.4000670
5 min	0.4014976	0.4001017	0.4000947	0.4003732
10 min	0.4027352	0.4003161	0.4002267	0.4006726
30 min	0.4081470	0.4010094	0.4003094	0.4017104

amount of λ, say, $\lambda = 10$ and $\lambda = 1000$ to test the performance of each estimator. Tables 4.1 - 4.6 show the simulation results of mean and standard deviation of the estimate σ with different types of estimators, different lengths of the time lag, and different values of λ in the Merton jump diffusion model, based on 1000 sample paths. Simulation results demonstrate that for the small magnitude of λ, both the BPV and TRV methods provide an accurate approximation of σ while the TRV estimators perform slightly better than the BPV estimator with the lower bias and the lower standard deviation. For the medium magnitude of λ, all of the TRV estimators give a better performance for the estimation accuracy than the BPV estimator. When the value of λ is extremely large, the BPV method generates an inaccurate estimation for the σ while the TRV estimators perform well only when the time lag is relatively small, say 1-minute observations.

For the Kou model, we use the following parameters:

$$\gamma = 0, \sigma = 0.4, p = 0.45, \eta_1 = 20, \eta_2 = 10, \lambda = 100.$$

Table 4.2
Standard deviation of the estimate σ for the Merton jump diffusion model with $\lambda = 10$ based on $K = 1000$ sample paths

Δ	$sd(\hat{\sigma}_{BPV})$	$sd(\hat{\sigma}_{TRV_{JT}})$	$sd(\hat{\sigma}_{TRV,2mc})$	$sd(\hat{\sigma}_{TRV,3mc})$
1 min	0.001048996	0.000898126	0.000896592	0.000935780
5 min	0.002444366	0.002027210	0.002021576	0.002077765
10 min	0.003561293	0.002875055	0.002952370	0.002871372
30 min	0.006852476	0.005068380	0.004851093	0.005306683

Table 4.3
Estimates of mean σ for the Merton jump diffusion model with $\lambda = 100$ based on $K = 1000$ sample paths

Δ	$\mathbb{E}(\hat{\sigma}_{BPV})$	$\mathbb{E}(\hat{\sigma}_{TRV_{JT}})$	$\mathbb{E}(\hat{\sigma}_{TRV,2mc})$	$\mathbb{E}(\hat{\sigma}_{TRV,3mc})$
1 min	0.4026951	0.4003905	0.4004464	0.4010029
5 min	0.4130809	0.4020334	0.4017282	0.4040007
10 min	0.4266889	0.4044699	0.4031553	0.4074626
30 min	0.48022305	0.4198294	0.4075378	0.4191378

Table 4.4
Standard deviation of the estimate σ for the Merton jump diffusion model with $\lambda = 100$ based on $K = 1000$ sample paths

Δ	$sd(\hat{\sigma}_{BPV})$	$sd(\hat{\sigma}_{TRV_{JT}})$	$sd(\hat{\sigma}_{TRV,2mc})$	$sd(\hat{\sigma}_{TRV,3mc})$
1 min	0.001093929	0.000887681	0.000898348	0.000948190
5 min	0.003124347	0.002066099	0.002125975	0.002175058
10 min	0.005351769	0.003242932	0.003081757	0.003389852
30 min	0.014070570	0.007122551	0.005832910	0.007954404

Table 4.5
Estimates of mean σ for the Merton jump diffusion model with $\lambda = 1000$ based on $K = 1000$ sample paths

Δ	$\mathbb{E}(\hat{\sigma}_{BPV})$	$\mathbb{E}(\hat{\sigma}_{TRV_{JT}})$	$\mathbb{E}(\hat{\sigma}_{TRV,2mc})$	$\mathbb{E}(\hat{\sigma}_{TRV,3mc})$
1 min	0.4266875	0.4047929	0.4052365	0.4108368
5 min	0.5332721	0.4480658	0.4220789	0.4564959
10 min	0.6669950	0.5603755	0.4471513	0.5722030
30 min	1.1998050	1.3426580	1.4360750	1.6497220

Table 4.6
Standard deviation of the estimate σ for the Merton jump diffusion model with $\lambda = 1000$ based on $K = 1000$ sample paths

Δ	$sd(\hat{\sigma}_{BPV})$	$sd(\hat{\sigma}_{TRV_{JT}})$	$sd(\hat{\sigma}_{TRV,2mc})$	$sd(\hat{\sigma}_{TRV,3mc})$
1 min	0.001631337	0.000997520	0.001007014	0.001158383
5 min	0.007503994	0.004467117	0.003380462	0.005934271
10 min	0.014275300	0.012720910	0.007528949	0.026463500
30 min	0.037987030	0.052139060	0.080948160	0.049380530

Table 4.7
Estimates of mean σ for the Kou model with $\lambda = 10$ based on $K = 1000$ sample paths

Δ	$\mathbb{E}(\hat{\sigma}_{BPV})$	$\mathbb{E}(\hat{\sigma}_{TRV_{JT}})$	$\mathbb{E}(\hat{\sigma}_{TRV,2mc})$	$\mathbb{E}(\hat{\sigma}_{TRV,3mc})$
1 min	0.4017137	0.3999157	0.4000129	0.4000358
5 min	0.4038536	0.3999938	0.4001008	0.4001582
10 min	0.4055322	0.4001783	0.4002706	0.4002709
30 min	0.4092282	0.4009466	0.4005650	0.4011437

Similar to the Merton model, we also believe that the jump intensity λ has a significant effect on the accuracy of integrated volatility estimation, so we test the performance of each estimator when $\lambda = 10$ and $\lambda = 1000$. Tables 4.7 - 4.12 show the simulation results of mean and standard deviation of the estimate σ with different types of estimators, different lengths of the time lag, and different values of λ in the Kou model, based on 1000 sample paths. Simulation results in the Kou model show similar behaviors of both BPV and TRV estimator in the Merton model. Hence, for the general jump diffusion model, we can conclude that both the length of time lag and the value of λ can significantly affect the accuracy of the BPV and TRV estimators.

For the variance gamma model, we use the following parameters:

$$\gamma = 0, \sigma = 0.4, \mu^{JMP} = 0, \sigma^{JMP} = 3\sqrt{\Delta}, \kappa = 0.3.$$

We use the *rgamma* function in R with parameters $\alpha = \Delta/k$ and $\beta = k$ to model a variance gamma process. We also conduct simulation experiments for the BPV and TRV methods with different magnitudes of κ, i.e. $\kappa = 5$ and $\kappa = 10$, to determine how the parameter κ could affect the performances of the BPV and TRV estimators. Tables 4.13

Table 4.8
Standard deviation of the estimate σ for the Kou model with $\lambda = 10$ based on $K = 1000$ sample paths

Δ	$sd(\hat{\sigma}_{BPV})$	$sd(\hat{\sigma}_{TRV_{JT}})$	$sd(\hat{\sigma}_{TRV,2mc})$	$sd(\hat{\sigma}_{TRV,3mc})$
1 min	0.001399656	0.000906607	0.000912244	0.000908262
5 min	0.003096891	0.002011597	0.002045633	0.002034037
10 min	0.004499415	0.002961821	0.002826675	0.002917857
30 min	0.007809922	0.004933537	0.004979540	0.005090971

Table 4.9
Estimates of mean σ for the Kou model with $\lambda = 100$ based on $K = 1000$ sample paths

Δ	$\mathbb{E}(\hat{\sigma}_{BPV})$	$\mathbb{E}(\hat{\sigma}_{TRV_{JT}})$	$\mathbb{E}(\hat{\sigma}_{TRV,2mc})$	$\mathbb{E}(\hat{\sigma}_{TRV,3mc})$
1 min	0.4175624	0.3999956	0.4000030	0.4001569
5 min	0.4386807	0.4010464	0.4006692	0.4018527
10 min	0.4536621	0.4035366	0.4017025	0.4046407
30 min	0.4893509	0.4192595	0.4073376	0.4175989

Table 4.10
Standard deviation of the estimate σ for the Kou model with $\lambda = 100$ based on $K = 1000$ sample paths

Δ	$sd(\hat{\sigma}_{BPV})$	$sd(\hat{\sigma}_{TRV_{JT}})$	$sd(\hat{\sigma}_{TRV,2mc})$	$sd(\hat{\sigma}_{TRV,3mc})$
1 min	0.003614369	0.000918461	0.000905486	0.000870944
5 min	0.008333235	0.002143654	0.002038793	0.002125001
10 min	0.012786210	0.003145236	0.002991145	0.003315278
30 min	0.018909920	0.007374914	0.006036465	0.006848706

Table 4.11
Estimates of mean σ for the Kou model with $\lambda = 1000$ based on $K = 1000$ sample paths

Δ	$\mathbb{E}(\hat{\sigma}_{BPV})$	$\mathbb{E}(\hat{\sigma}_{TRV_{JT}})$	$\mathbb{E}(\hat{\sigma}_{TRV,2mc})$	$\mathbb{E}(\hat{\sigma}_{TRV,3mc})$
1 min	0.578044	0.4030258	0.4000849	0.4018460
5 min	0.7881979	0.4783682	0.4070876	0.4222199
10 min	0.9416258	0.6350743	0.4232592	0.4715833
30 min	1.2870130	1.2226040	0.7495642	1.4634190

Table 4.12
Standard deviation of the estimate σ for the Kou model with $\lambda = 1000$ based on $K = 1000$ sample paths

Δ	$sd(\hat{\sigma}_{BPV})$	$sd(\hat{\sigma}_{TRV_{JT}})$	$sd(\hat{\sigma}_{TRV,2mc})$	$sd(\hat{\sigma}_{TRV,3mc})$
1 min	0.020834210	0.001115822	0.000928850	0.000965472
5 min	0.036105670	0.010873010	0.002607768	0.003895576
10 min	0.044966500	0.025763230	0.005210286	0.010401160
30 min	0.056189070	0.059977140	0.092506880	0.110675700

Table 4.13
Estimates of mean σ for the variance gamma model with $\kappa = 0.3$ based on $K = 1000$ sample paths

Δ	$\mathbb{E}(\hat{\sigma}_{BPV})$	$\mathbb{E}(\hat{\sigma}_{TRV_{JT}})$	$\mathbb{E}(\hat{\sigma}_{TRV,2mc})$	$\mathbb{E}(\hat{\sigma}_{TRV,3mc})$
1 min	0.4000466	0.4000313	0.4000758	0.4000575
5 min	0.4002446	0.4001313	0.4002004	0.4002807
10 min	0.4006318	0.4003963	0.4002650	0.4005396
30 min	0.4018848	0.4011953	0.4009165	0.4016706

Table 4.14
Standard deviation of the estimate σ for the variance gamma model with $\kappa = 0.3$ based on $K = 1000$ sample paths

Δ	$sd(\hat{\sigma}_{BPV})$	$sd(\hat{\sigma}_{TRV_{JT}})$	$sd(\hat{\sigma}_{TRV,2mc})$	$sd(\hat{\sigma}_{TRV,3mc})$
1 min	0.001049615	0.000929353	0.000914680	0.000909218
5 min	0.002370896	0.002029259	0.001950724	0.002044569
10 min	0.003256612	0.002774886	0.002880630	0.002825606
30 min	0.005663113	0.004961795	0.005149247	0.005000513

- 4.18 present the simulation results of mean and standard deviation of the estimate σ with different types of threshold sequences, different lengths of the time lag, and different magnitudes of κ for the variance gamma model, based on 1000 sample paths.

In the normal inverse Gaussian model, we use the same parameters as those used in the variance gamma process. We use the *rinvgauss* function in R with parameters $\mu = \Delta$ and $\lambda = \Delta^2/\kappa$ to generate independent inverse Gaussian variables. Tables 4.19 - 4.24 demonstrate the simulation results of mean and standard deviation of the estimate σ

Table 4.15
Estimates of mean σ for the variance gamma model with $\kappa = 5$ based on $K = 1000$ sample paths

Δ	$\mathbb{E}(\hat{\sigma}_{BPV})$	$\mathbb{E}(\hat{\sigma}_{TRV_{JT}})$	$\mathbb{E}(\hat{\sigma}_{TRV,2mc})$	$\mathbb{E}(\hat{\sigma}_{TRV,3mc})$
1 min	0.4000096	0.3999851	0.4000085	0.4000132
5 min	0.4001027	0.3999501	0.3999762	0.3999920
10 min	0.4001925	0.4000911	0.3998073	0.4000855
30 min	0.4007118	0.4000899	0.3997050	0.4000876

Table 4.16
Standard deviation of the estimate σ for the variance gamma model with $\kappa = 5$ based on $K = 1000$ sample paths

Δ	$sd(\hat{\sigma}_{BPV})$	$sd(\hat{\sigma}_{TRV_{JT}})$	$sd(\hat{\sigma}_{TRV,2mc})$	$sd(\hat{\sigma}_{TRV,3mc})$
1 min	0.001010473	0.000913089	0.000898929	0.000882976
5 min	0.002283857	0.002018694	0.002063001	0.002023413
10 min	0.003297748	0.002812975	0.002832983	0.002872297
30 min	0.005894798	0.004906396	0.004782640	0.004809131

Table 4.17
Estimates of mean σ for the variance gamma model $\kappa = 10$ based on $K = 1000$ sample paths

Δ	$\mathbb{E}(\hat{\sigma}_{BPV})$	$\mathbb{E}(\hat{\sigma}_{TRV_{JT}})$	$\mathbb{E}(\hat{\sigma}_{TRV,2mc})$	$\mathbb{E}(\hat{\sigma}_{TRV,3mc})$
1 min	0.4000565	0.3999941	0.4000038	0.3999585
5 min	0.3999309	0.3999967	0.3999415	0.4000038
10 min	0.4001871	0.4000174	0.3999429	0.3998717
30 min	0.4004741	0.4000832	0.3997814	0.3998473

Table 4.18
Standard deviation of the estimate σ for the variance gamma model $\kappa = 10$ based on $K = 1000$ sample paths

Δ	$sd(\hat{\sigma}_{BPV})$	$sd(\hat{\sigma}_{TRV_{JT}})$	$sd(\hat{\sigma}_{TRV,2mc})$	$sd(\hat{\sigma}_{TRV,3mc})$
1 min	0.001020625	0.000928131	0.000902287	0.000917221
5 min	0.002301829	0.001988927	0.001971818	0.002040393
10 min	0.003301280	0.002869280	0.002847721	0.002991717
30 min	0.005830217	0.004874829	0.004878287	0.004956715

Table 4.19
Estimates of mean σ for the normal inverse Gaussian model with with $\kappa = 0.3$ based on $K = 1000$ sample paths

Δ	$\mathbb{E}(\hat{\sigma}_{BPV})$	$\mathbb{E}(\hat{\sigma}_{TRV_{JT}})$	$\mathbb{E}(\hat{\sigma}_{TRV,2mc})$	$\mathbb{E}(\hat{\sigma}_{TRV,3mc})$
1 min	0.4000466	0.4000593	0.4000239	0.4001214
5 min	0.4005031	0.4002616	0.4002638	0.4003656
10 min	0.4006063	0.4005682	0.4005319	0.4007256
30 min	0.4018123	0.4018078	0.4011529	0.4019086

Table 4.20
Standard deviation of the estimate σ for the normal inverse Gaussian model with $\kappa = 0.3$ based on $K = 1000$ sample paths

Δ	$sd(\hat{\sigma}_{BPV})$	$sd(\hat{\sigma}_{TRV_{JT}})$	$sd(\hat{\sigma}_{TRV,2mc})$	$sd(\hat{\sigma}_{TRV,3mc})$
1 min	0.001050124	0.000901176	0.0008797061	0.0009326041
5 min	0.002327431	0.002047176	0.001987792	0.002058507
10 min	0.003281180	0.002842009	0.002824205	0.002921731
30 min	0.005792352	0.005057107	0.005232538	0.005233086

with different types of threshold sequences, different lengths of the time lag, and different values of κ for the normal inverse Gaussian model, based on 1000 sample paths.

Comparing the results of the mean and standard deviation estimates in the variance gamma model and the normal inverse Gaussian model, both the BPV and TRV estimators perform well in general. The threshold type estimators ($\hat{\sigma}_{TRV_{JT}}, \hat{\sigma}_{TRV,2mc}, \hat{\sigma}_{TRV,3mc}$) are slightly superior to the BPV estimator because of the lower bias and the lower standard deviation. The three threshold variations type estimators with different types of thresh-

Table 4.21
Estimates of mean σ for the normal inverse Gaussian model with $\kappa = 5$ based on $K = 1000$ sample paths

Δ	$\mathbb{E}(\hat{\sigma}_{BPV})$	$\mathbb{E}(\hat{\sigma}_{TRV_{JT}})$	$\mathbb{E}(\hat{\sigma}_{TRV,2mc})$	$\mathbb{E}(\hat{\sigma}_{TRV,3mc})$
1 min	0.4000767	0.4000274	0.4000228	0.4000314
5 min	0.4000737	0.3999147	0.4000516	0.4000585
10 min	0.4003362	0.3999816	0.4001046	0.4001495
30 min	0.4008925	0.4005720	0.4002601	0.4003704

Table 4.22
Standard deviation of the estimate σ for the normal inverse Gaussian model with $\kappa = 5$ based on $K = 1000$ sample paths

Δ	$sd(\hat{\sigma}_{BPV})$	$sd(\hat{\sigma}_{TRV_{JT}})$	$sd(\hat{\sigma}_{TRV,2mc})$	$sd(\hat{\sigma}_{TRV,3mc})$
1 min	0.001041723	0.000882914	0.000865751	0.000897367
5 min	0.002262593	0.002105065	0.001956236	0.002017366
10 min	0.003383207	0.002879882	0.002814585	0.002866610
30 min	0.005620133	0.004888543	0.005112446	0.004955696

Table 4.23
Estimates of mean σ for the normal inverse Gaussian model with $\kappa = 10$ based on $K = 1000$ sample paths

Δ	$\mathbb{E}(\hat{\sigma}_{BPV})$	$\mathbb{E}(\hat{\sigma}_{TRV_{JT}})$	$\mathbb{E}(\hat{\sigma}_{TRV,2mc})$	$\mathbb{E}(\hat{\sigma}_{TRV,3mc})$
1 min	0.4000706	0.3999592	0.4000414	0.4000163
5 min	0.4000517	0.4000291	0.4000045	0.4001106
10 min	0.4003102	0.4000295	0.3999737	0.4000773
30 min	0.4005513	0.4003727	0.4000553	0.4002520

Table 4.24
Standard deviation of the estimate σ for the normal inverse Gaussian model with $\kappa = 10$ based on $K = 1000$ sample paths

Δ	$sd(\hat{\sigma}_{BPV})$	$sd(\hat{\sigma}_{TRV_{JT}})$	$sd(\hat{\sigma}_{TRV,2mc})$	$sd(\hat{\sigma}_{TRV,3mc})$
1 min	0.001040547	0.000906029	0.000915585	0.000878416
5 min	0.002407645	0.002061733	0.002076517	0.002060894
10 min	0.003378147	0.002834031	0.002838745	0.002915124
30 min	0.005949271	0.005031785	0.005238048	0.004866423

old sequences have similar performances in these two models. In addition, the kurtosis parameter κ does not significantly affect the accuracy of integrated volatility estimation. Hence, in the Lévy models building by Brownian subordination, the length of time lag is the key factor of the accuracy of the estimation. With a smaller length of time lag, the estimated results are more accurate.

5. Conclusions

In this paper, we aim to explore the performances of the BPV and TRV estimators for jump detection and integrated volatility estimation. To do so, we first construct four types of Lévy stochastic process models: the Merton jump diffusion model, the Kou model, the variance gamma model and the normal inverse Gaussian model, which have the same diffusion parts of Brownian motion but different types of jump component. We then study further the mechanism of jump detection for high-frequency data through the BPV method and the TRV method. Additionally, we also introduce some types of threshold sequences for threshold type estimators, which may affect the efficiency of jump detection. Finally, we apply these two methods into simulated high-frequency data in different models with different time lags and test the accuracy of integrated volatility estimation.

Based on the simulated data, the estimations generated by the TRV method have the lower bias and the lower variance than the estimations obtained through the BPV method, which indicates that threshold type estimators perform better on the efficiency of jump detection and provide more accurate estimations for the integrated volatility. We also find that the estimations are more accurate when dividing a fixed time horizon into shorter time intervals. Thus, the length of time interval have much influence on the integrated volatility estimation. In addition, for the general jump diffusion model, the intensity of jumps λ also has some effects on the integrated variance estimation, which

indicates the adaptability property is not satisfied for all parameter settings. For the Lévy processes building by Brownian subordination, the kurtosis parameter κ does not affect much on the integrated volatility estimation.

In the end, the TRV method provides a better and more precise estimator for the integrated volatility estimation, which could help investors to forecast the market volatility and avoid the investment risks in the financial system. There are still some limitations in our work, since we only apply the BPV and TRV methods and test their performances in simulated high-frequency data. Further studies should be conducted to show how suitable these two methods are for integrated volatility estimation in the real financial world.

REFERENCES

[1] Robert C Merton. Option pricing when underlying stock returns are discontinuous. *Journal of financial economics*, 3(1-2):125–144, 1976.

[2] Steven G Kou. A jump-diffusion model for option pricing. *Management science*, 48(8):1086–1101, 2002.

[3] Dilip B Madan and Eugene Seneta. The variance gamma (vg) model for share market returns. *Journal of business*, pages 511–524, 1990.

[4] Ole E Barndorff-Nielsen. Processes of normal inverse gaussian type. *Finance and stochastics*, 2(1):41–68, 1997.

[5] Peter Tankov. *Financial modelling with jump processes*, volume 2. CRC press, 2003.

[6] Ole E Barndorff-Nielsen and Neil Shephard. Power and bipower variation with stochastic volatility and jumps. *Journal of financial econometrics*, 2(1):1–37, 2004.

[7] José E Figueroa-López and Jeffrey Nisen. Second-order properties of thresholded realized power variations of fja additive processes. *Preprint, available at https://pages. wustl. edu/figueroa/publications*, 2016.

[8] Cecilia Mancini. Disentangling the jumps of the diffusion in a geometric jumping brownian motion. *Giornale dellIstituto Italiano degli Attuari*, 64(19-47):44, 2001.

[9] Cecilia Mancini. Estimation of the characteristics of the jumps of a general poisson-diffusion model. *Scandinavian Actuarial Journal*, 2004(1):42–52, 2004.

[10] Jean Jacod, Viktor Todorov, et al. Efficient estimation of integrated volatility in presence of infinite variation jumps. *The Annals of Statistics*, 42(3):1029–1069, 2014.

[11] José E Figueroa-López and Cecilia Mancini. Optimum thresholding using mean and conditional mean square error. *arXiv preprint arXiv:1708.04339*, 2017.

[12] José E Figueroa-López and Jeffrey Nisen. Optimally thresholded realized power variations for lévy jump diffusion models. *Stochastic Processes and their Applications*, 123(7):2648–2677, 2013.